Concerted Motion of a Protein−Peptide Complex: Backbone Dynamics Studies of an ^{15}N-Labeled Peptide Derived from P^{21}-Activated Kinase Bound to Cdc42Hs·GMPPCP†

Dawit Gizachew and Robert E. Oswald*

Department of Molecular Medicine, Cornell University, Ithaca, New York 14853

Received May 15, 2001; Revised Manuscript Received September 26, 2001

ABSTRACT: Cdc42Hs is a member of the Ras superfamily of GTPases which, when active, initiates a cascade beginning with the activation of several kinases, including P^{21}-activated kinase (PAK). We previously determined the structure of a complex between a 46 amino acid fragment peptide derived from the PAK binding domain (PBD46) and Cdc42Hs·GMPPCP (Gizachew, D., Guo, W., Chohan, K. K., Sutcliffe, M. J., and Oswald, R. E. (2000) *Biochemistry 39*, 3963−3971). Previous studies (Loh, A. P., Guo, W., Nicholson, L. K., and Oswald, R. E. (1999) *Biochemistry 38*, 12547−12557) suggest that the regions of Cdc42Hs that bind effectors and regulators have distinct dynamic properties from the remainder of the protein. Here, we describe the backbone dynamics of PBD46 bound to Cdc42Hs·GMPPCP. T_1, T_2, $T_{1\rho}$, and steady-state nuclear Overhauser effects were measured at 500 and 600 MHz. An extension of the Lipari−Szabo model-free analysis was used to determine the order parameters (S^2) and local correlation times (τ_e) of the N−H bond vectors within PBD46. Both Cdc42Hs and PBD46 exhibit increased mobility in the free versus the bound state, suggesting that protein flexibility may be required for high-affinity PBD46 binding and, presumably, the activation of PAK. Different backbone dynamics were observed in different regions of the peptide. The β-strand region of bound PBD46, which makes contacts with β2 of Cdc42Hs, exhibits low mobility on the pico- to nanosecond timescale. However, the part of PBD46 that interacts with Switch I of Cdc42Hs exhibits greater mobility. Thus, PBD46 and Cdc42Hs form a tight complex that exhibits concerted dynamics.

The members of the Ras superfamily of low molecular weight GTP binding proteins (G proteins) are involved in a number of diverse biological processes, including cell growth, differentiation, cytoskeletal organization, membrane and protein trafficking, and secretion (*1*). G proteins are molecular switches that play important roles in a variety of signal-transduction pathways. Their biochemical activities are determined by the nature of the guanine nucleotide (either GDP[1] or GTP) that is bound to the active site. When bound to GTP (or GTP analogues), G proteins are active and capable of mediating specific biochemical reactions or binding events. They remain in this state until the GTP is hydrolyzed to GDP by the intrinsic GTPase activity of the protein. The levels of the active (GTP-bound) and inactive (GDP-bound) protein are regulated by interactions with regulatory proteins, such as GTPase activating proteins (GAPs), which increase the GTPase activity, guanine nucleotide exchange factors (GEFs), which catalyze the exchange of GDP for GTP, and guanine nucleotide dissociation inhibitors (GDIs), which inhibit the dissociation of nucleotide. The most extensively studied member of the Ras superfamily is Ras P^{21}. This protein is found in almost all cell types; single amino acid mutations of the ras genes are found in approximately 30% of human tumors and thus constitute the most prevalent oncogene in human carcinogenesis (*2*).

One subfamily of Ras-like proteins is the Rho subfamily. Members of the Rho subfamily (including Cdc42Hs, Rho, and Rac) play important roles in the regulation of cell proliferation, differentiation, and cytoskeletal organization by binding to different effectors, which initiate a cascade of protein−protein interactions (*1*). A variety of effectors have been identified and include the p85 subunit of the PI3 kinase (*3*), the Wiskott−Aldrich syndrome protein (WASP; *4*), the ACK tyrosine kinase (*5*), and the P^{21}-activated serine/threonine kinase (PAK; *6*, *7*). In several cases (e.g., WASP, ACK, and PAK), effectors have a common region called the CRIB (Cdc42Hs-Rac interactive binding) domain (*8*).

Interaction of Cdc42Hs with PAK initiates a cascade of kinase interactions, which leads to the activation of the nuclear stress-responsive MAP kinases, JNK1, and p38.

† This work was supported by Grant R01 GM56233 from the National Institutes of Health.

* To whom correspondence should be addressed at Department of Molecular Medicine, Cornell University. Phone: 1-607-253-3877. Fax: 1-607-253-3659. E-mail: reo1@cornell.edu.

[1] Abbreviations: GDP, guanosine-5′-diphosphate; GTP, guanosine-5′-triphosphate; GMPPCP, β,γ-methylene derivative of GTP; GST, glutathione S-transferase; PBD46, 46 amino acid portion of the Cdc42Hs binding domain on PAK; PAK, P^{21}-activated kinase; GEF, guanine nucleotide exchange factor; GAP, GTPase activating protein; GDI, guanine nucleotide dissociation inhibitor; Switch I, residues 31−40 on Cdc42Hs; Switch II, residues 57−74 on Cdc42Hs; HSQC, heteronuclear single quantum correlation; NMR, nuclear magnetic resonance; T_1, longitudinal relaxation time; T_2, transverse relaxation time; $T_{1\rho}$, longitudinal relaxation time in the rotating frame; NOE, nuclear Overhauser effect; ACK, ACK tyrosine kinase that interacts with Cdc42Hs; fACK, residues 504−545 of ACK tyrosine kinase; WASP, Wiskott−Aldrich syndrome protein; WASP−GBD, residues 230−288 of WASP that bind to Cdc42Hs.

10.1021/bi010989h CCC: $20.00
Published on Web 11/02/2001

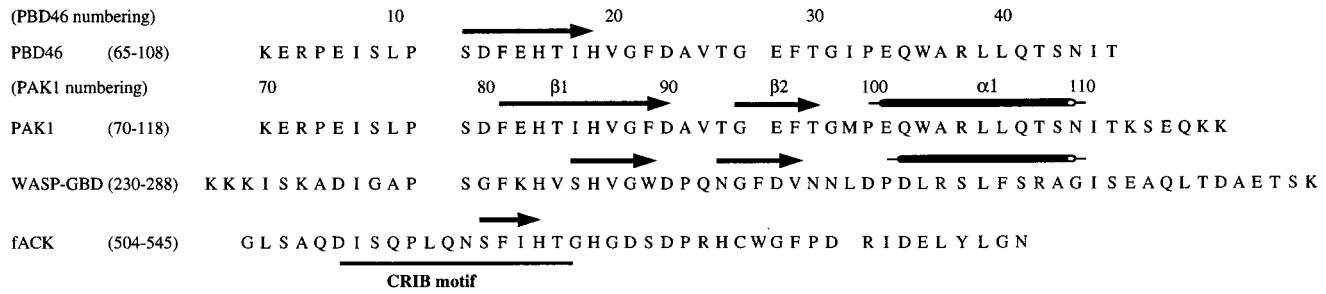

FIGURE 1: Sequence alignment of PBD46 and peptides derived from PAK1 (*18*), ACK (*19*), and WASP (*20*). Numbering shown is that for the intact proteins. For PBD46, both the protein and the peptide (as used in the text) numberings are shown. The CRIB sequence is underlined, and secondary structures are indicated by an arrow for a β strand and by a cylinder for a helix.

PAKs are members of a family of serine/threonine protein kinases, and so far, four PAK (PAK1−4) subtypes have been identified in mammals (*9, 10*). These are classified by their interaction with the small GTPases, Cdc42Hs, and Rac. PAK1−3 have an N-terminal half that includes autoregulatory and interaction segments and a C-terminal kinase domain. The crystal structure of a PAK1 dimer has been determined (*11*). In the inactive state, the inhibitory switch domain of PAK1 positions a polypeptide segment across the kinase cleft, and it has been suggested that GTPase binding results in the conformational rearrangement of the inhibitory switch domain which leads to activation of the enzyme. A 46 amino acid peptide (PBD46), which binds Cdc42Hs ($K_D \approx 16$ nM), was derived from the PAK1 dimerization domain (*12*). This PBD46 construct includes the CRIB motif that is required for Cdc42Hs binding and has shown a high affinity for Cdc42Hs compared to other shorter constructs of PAK binding domains (*12*). However, the binding affinity of PBD46 is similar to that of longer constructs of PAK such as PBD74 (which has an additional 28 amino acids at the C terminus of PBD46; *12*). The NMR structure of the complex between Cdc42Hs and PBD46 has been determined (*13*), revealing that, while PBD46 is unstructured and highly mobile in its free form, PBD46 becomes structured when it is bound to Cdc42Hs. Cdc42Hs also shows complex internal motion (particularly in the regions termed Switch I and Switch II) when unbound, but upon binding to PBD46, the degree of motional complexity is reduced (*14*).

While information on the three-dimensional structure of the Cdc42Hs−PBD46 complex (*13*) has thrown light on the finer details of the interactions between the two proteins, it has been suggested that many of the regulatory functions and mechanisms may be subtly dependent on the dynamic properties of both Cdc42Hs and PAK (*14, 15*). In this work, the backbone dynamics of PBD46 while bound to Cdc42Hs have been studied by expressing and purifying ^{15}N-labeled PBD46 and natural abundance Cdc42Hs. The extended Lipari−Szabo model-free order parameters and local correlation times were derived using measurements of NMR relaxation parameters. PBD46 was found to have several regions with distinct backbone dynamics that correlate with specific regions of the binding interface and with the backbone dynamics of Cdc42Hs in those regions.

EXPERIMENTAL PROCEDURES

Protein Preparation and Purification. The details of cell growth and protein purification for Cdc42Hs have been described previously (*12*). Briefly, unlabeled Cdc42Hs is expressed as a hexahistidine-tagged protein in *Escherichia coli* strain BL21(DE3) from pET-15b-Cdc42Hs. This expression plasmid was subcloned to include the 178 N-terminal amino acids (and a glycine, serine, and histidine which occurs before the starting methionine) from the original pGEX-Cdc42Hs expression plasmid (*16*) to improve the yield and to remove the unstructured C-terminal tail. The Cdc42Hs construct as expressed is bound to GDP so that the protein is in its inactive form. To activate Cdc42Hs, GDP was exchanged for GMPPCP (which is a nonhydrolyzable analogue of GTP; one molecule of GMPPCP binds one molecule of Cdc42Hs), using the protocol described by John et al. (*17*). Each Cdc42Hs·GMPPCP (active form) molecule binds one molecule of PBD46.

The expression and purification of PBD46 have also been reported previously (*12*). Briefly, the ^{15}N-labeled and GST-fused PBD46 peptide was expressed in 2 × M9 medium using ^{15}N-labeled NH_4Cl as the sole source of ^{15}N. After the glutathione S-transferase (GST)-fused PBD46 was extracted from the cells, the GST−PBD46 protein was purified using a GST affinity column, and later was eluted from the affinity column with 10 mM GSH in a 20 mM Tris-HCl (pH = 8) buffer. The GST was cleaved from PBD46 by adding thrombin and incubating for 12 h. The completeness of the cleavage was confirmed by PAGE on a 10% SDS gel. The ^{15}N-labeled PBD46 was mixed with natural abundance Cdc42Hs·GMPPCP and incubated at 4 °C for 12 h. The complex was then dialyzed to exchange the Tris-HCl buffer with an NMR buffer (25 mM NaCl, 5 mM NaH_2PO_4, 5 mM $MgCl_2$, and 1 mM NaN_3, pH = 5.5). Unbound PBD46 was separated from bound PBD46 using a Superdex-75 (Pharmacia) sizing column. The sequence alignments of PBD46 with peptides derived from PAK1 (*18*), ACK (*19*), and WASP (*20*) are shown in Figure 1.

NMR Spectroscopy. Samples of both the Cdc42Hs·GMPPCP−PBD46 complex and free PBD46 were prepared at approximately 0.5 mM in an NMR buffer with 10% D_2O. Spectra were obtained on Varian Inova 600 MHz (Cornell Biomolecular NMR center) and Varian Unity 500 MHz (Cornell Chemistry NMR facility) spectrometers. Both spectrometers were equipped with triple-resonance pulsed-field gradient probes. Spectra were obtained at 25 °C in the States-TPPI mode (*21, 22*) for quadrature detection. Carrier frequencies for ^{1}H and ^{15}N were 4.75 and 118.42 ppm, respectively.

Data were processed using NMRPipe version 1.6 on a Sun Ultra 5 workstation. Sensitivity-enhanced experiments were preprocessed (*23*) and were zero-filled to double the original

data points. The data were apodized with a Gaussian window function. Numerical solvent suppression was applied prior to Fourier transformation, and a polynomial function was applied for baseline correction after Fourier transformation. Spectra were visualized and peaks picked using the PIPP macro (version 4.3.1) assignment programs (*24*).

T_1, T_2, and $T_{1\rho}$ values were measured with sensitivity enhancement using 128 × 512 real data points at 16 scans per point, using pulse sequences described elsewhere (*25*, *26*). $T_{1\rho}$ data were obtained using continuous ^{15}N spin locking (*27*). Twelve relaxation data points were used to define each decay curve, and delay times were in the range of 12−1102 ms for T_1, 16−150 ms for T_2, and 8−96 ms for $T_{1\rho}$. Peak volumes were determined by fitting a Gaussian line shape to the experimental peaks using the program nlinLS (*24*). Relaxation times (T_1, T_2, and $T_{1\rho}$) were then obtained using conjugate gradient minimization and Monte Carlo simulation to fit the relaxation delay points to an exponential decay function (*28*). Errors in the relaxation times were chosen as the larger of those from the relaxation fit or from replicates of measured relaxation delay peak volumes (the average of the standard deviations of two or three (in most cases) sets of replicates).

$T_{1\rho}$ values were corrected for off-resonance effects using the following equations (*29*):

$$\frac{1}{T_2} = \frac{1}{T_{1\rho}}\csc^2\theta - \frac{1}{T_1}\cot^2\theta \quad (1)$$

$$\theta = \arctan\left(\frac{B_0\Delta\delta}{B_1}\right) \quad (2)$$

where θ is the tip angle, B_0 is the stationary magnetic field, B_1 is the spin-lock field strength (2.5 kHz), and $\Delta\delta$ is the chemical shift offset from the carrier frequency of ^{15}N. For the nuclear Overhauser effects (NOEs), the ratio of the integrated cross peaks of the ^{1}H−^{15}N heteronuclear NOE spectra was calculated from the equation

$$\text{NOE} = V_{\text{sat}}/V_{\text{no sat}} \quad (3)$$

where V_{sat} and $V_{\text{no sat}}$ are the volumes of a given peak from the spectra collected with and without proton saturation, respectively. Three sets of data (with and without proton saturation) were obtained. The nine possible combinations of NOE values were calculated, and the standard deviation was used as the uncertainty in the measurement. Because only one set of NOE data for the free PBD46 was obtained, standard deviations in the NOE values were determined from the root-mean-square baseline noise as described by Nicholson et al. (*30*).

Theory and Data Analysis. The major relaxation mechanisms in ^{1}H−^{15}N heteronuclear relaxation experiments are the dipolar coupling between the amide ^{15}N nucleus and that of the attached proton and the chemical shift anisotropy of ^{15}N. The measurable relaxation parameters (T_1, longitudinal relaxation; T_2, transverse relaxation; steady-state NOE) can be related to the spectral density function ($J(\omega)$) which, in turn, depends on the dynamics parameters (eq 4). The expression for T_2 includes a chemical-exchange term (R_{ex}), which is dependent upon the field strength (*31*). Thus, collecting data at more than one field strength is of value for determining the contribution of the chemical exchange to the dynamics parameters.

Table 1: Models Used in the Analysis of Backbone Dynamics

model	fit parameters	assumptions[a]
1	S^2	$S^2 = 1$, $\tau_f \rightarrow 0$, $\tau_s \rightarrow 0$, $R_{ex} = 0$
2	S^2 and τ_e	$S^2 = 1$, $\tau_e < \tau_m$, $R_{ex} = 0$
3	S^2 and R_{ex}	$S^2 = 1$, $\tau_f \rightarrow 0$, $\tau_s \rightarrow 0$
4	S^2, τ_e, and R_{ex}	$S^2 = 1$, $\tau_e < \tau_m$
5	S_s^2, S_f^2, and τ_e	$\tau_f \rightarrow 0$, $\tau_e < \tau_m$, $R_{ex} = 0$

[a] For models 1, 3, and 5, τ_f is assumed to be sufficiently fast as to make a negligible contribution to the relaxation parameters. In models 2 and 4, the slow component is absent and $\tau_f = \tau_e$. In models 1−4, $S^2 = S_f^2$. Models 3 and 4 are derived from models 1 and 2, respectively, by including a nonzero chemical-exchange contribution, R_{ex}, in the relaxation model to accommodate chemical-exchange and other pseudo-first-order processes that contribute to the decay of the transverse magnetization on timescales slower than the overall correlation time, τ_m.

The spectral density function can be related to the amplitudes and timescales of the internal motions through order parameters (S^2) and local correlation times (τ_e), using an approach pioneered by Lipari and Szabo (*32*) and later extended by Clore et al. (*33*).

$$J(\omega) = \frac{2}{5}\left[\frac{S^2\tau_m}{1+(\omega\tau_m)^2} + \frac{(1-S_f^2)\tau_f'}{1+(\omega\tau_f')^2} + \frac{(S_f^2-S^2)\tau_s'}{1+(\omega\tau_s')^2}\right] \quad (4)$$

for which

$$\frac{1}{\tau_i'} = \frac{1}{\tau_i} + \frac{1}{\tau_m} \quad (5)$$

where ω is the Larmor frequency of the ^{15}N nucleus and τ_i is the local correlation time on either the fast (f) or slow (s) timescale relative to τ_m ($\tau_f < \tau_s < \tau_m$), the molecular correlation time. $S^2 = S_s^2S_f^2$ is the square of the generalized order parameter characterizing the amplitude of the internal motions of each N−H bond, and S_f^2 and S_s^2 are the squares of the order parameters for the internal motions on the fast (τ_f) and slow (τ_s) timescales, respectively. The value of S^2 ranges between 0 (unrestricted isotropic motion) and 1 (completely restricted motion).

Previous studies (*14*, *15*) have shown that the Cdc42Hs·GMPPCP−PBD46 complex exhibits isotropic molecular motion with $\tau_m = 18.6$ ns at 25 °C. Using an isotropic model, the values of the parameters that characterize the residue-specific (S_f^2, S_s^2, τ_e, and R_{ex}) dynamics of PBD46 were obtained by fitting the relaxation data to five different dynamic models (Table 1) at two field strengths, while holding the value of τ_m fixed, using the program ModelFree (version 4; *34*) as described previously (*14*). The most appropriate model for each residue was chosen on the basis of the nested *F*-test criterion, which takes into account the varying number of degrees of freedom in the different models (*34*).

RESULTS

Relaxation Data. The ^{1}H−^{15}N HSQC spectrum of free PBD46 (Figure 2A) is poorly dispersed in the proton dimension, indicating that the peptide is not well structured. In contrast, the well-dispersed spectrum of bound PBD46 (Figure 2B) is consistent with a highly structured peptide.

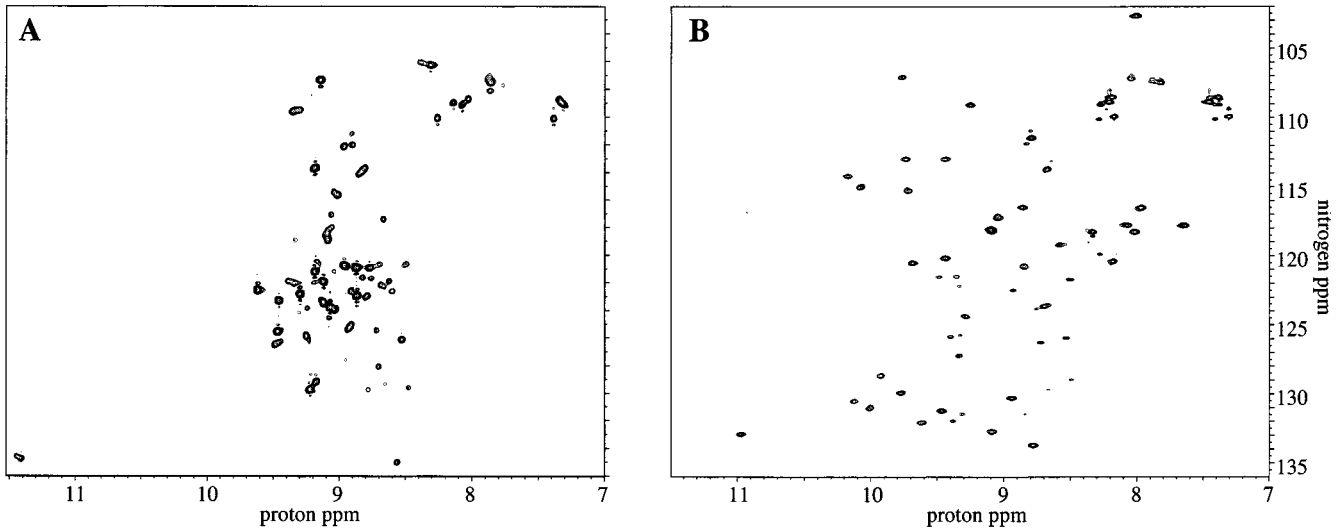

FIGURE 2: $^{1}H-^{15}N$ HSQC spectra of **(**A**)** free PBD46 and **(**B**)** PBD46 bound to Cdc42Hs·GMPPCP. Only PBD46 is uniformly ^{15}N-labeled; therefore, Cdc42Hs resonances do not appear in the spectrum. In addition to $^{1}H-^{15}N$ backbone correlations, several side-chain amide resonances appear on the spectra. Both spectra were obtained at 600 MHz.

Table 2: Average Values of Relaxation Parameters with Standard Errors of the Mean for Bound and Free PBD46

600 MHz	T_1 (s)	T_2 from $T_{1\rho}$ (ms)	T_2 (ms)	NOE	S^2
N and C termini	0.96 ± 0.05	198 ± 39	202 ± 40	0.014 ± 0.146	0.235 ± 0.065[a]
residues 9−19	1.35 ± 0.03	54.8 ± 3.3	55.8 ± 0.9	0.728 ± 0.024	0.752 ± 0.033
residues 20−40	1.22 ± 0.02	60.7 ± 1.4	64.2 ± 4.5	0.633 ± 0.033	0.625 ± 0.027[a]
bound PBD46[b]	1.19 ± 0.03	91.7 ± 13.3	94.6 ± 13.6	0.511 ± 0.059	0.566 ± 0.038
free PBD46[b]	0.78 ± 0.02	367 ± 17		0.14 ± 0.02	
500 MHz	T_1 (s)	T_2 from $T_{1\rho}$ (ms)	500 MHz	T_1 (s)	T_2 from $T_{1\rho}$ (ms)
N and C termini	0.80 ± 0.04	238 ± 55	residues 20−40	0.99 ± 0.03	66.5 ± 4.9
residues 9−19	1.00 ± 0.03	55.6 ± 1.5	bound PBD46[b]	0.95 ± 0.02	104 ± 18

[a] Significantly different at the 0.01 level relative to residues 9−19 (ANOVA and Student's *t* test). [b] Average relaxation parameters for the entire peptide.

To assess the dynamics of PBD46, T_1, $T_{1\rho}$, T_2, and NOE values at 600 MHz and T_1 and $T_{1\rho}$ values at 500 MHz were determined for the bound form of PBD46; T_1, $T_{1\rho}$, T_2, and NOE values at 600 MHz were determined for the free form of PBD46. Sequence assignments of the backbone N−H resonances of bound PBD46 have been previously published (*13*). Four $^{1}H-^{15}N$ correlations were unassigned, including the first two residues in the peptide. A large error in the exponential decay fits precluded the use of residue 46 in the relaxation parameter analysis. Residue 46, the last residue of the peptide, may relax much more slowly than the rest of the amino acids because of its fast and complex motion, which reduces effective relaxation mechanisms. The average values (with standard errors of the mean) of the remaining relaxation data for both the free and bound PBD46 are shown in Table 2. The average T_1 and the NOE values are significantly lower and the average T_2 values are significantly higher for free PBD46 than for bound PBD46. This indicates that the free peptide is highly mobile as compared to bound PBD46.

Residue-specific T_1 values are shown in Figure 3A. The three regions of the bound peptide that were considered on the basis of the structure of the complex (*13*) exhibit differences in relaxation parameters. These include **(**1**)** N- and C-terminal residues ($T_1 = 0.96 \pm 0.05$ s), which have shorter T_1 values than the structured regions of the peptide, **(**2**)** residues 9−19, which form a β strand and have higher T_1 values (average $T_1 = 1.35 \pm 0.03$), and **(**3**)** residues 20−40, which contact Switches I and II and have average T_1 values that are slightly lower than residues 9−19 (average $T_1 = 1.22 \pm 0.02$).

Similarly, the different regions of the bound peptide clearly show different ranges of T_2 values (Figure 3B). Both the N and C termini exhibit relatively long T_2 values (up to 393 ms for residue 45 at 600 MHz) as compared to the average T_2 of 58.7 ± 1.1 ms for the remainder of the peptide. Furthermore, the average T_2 in the β-strand region is 54.8 ± 1.1 ms, while the average T_2 value in the region that contacts Switches I and II increases to 60.7 ± 1.4 ms. In particular, residue V25 has a particularly long T_2 (75.2 ms) for the structured regions of PBD46. The variation of T_2 in the different parts of the peptide has been observed in both the $T_{1\rho}$ and T_2 experiments. As shown in Table 2, the average T_2 values derived from $T_{1\rho}$ are not significantly different from those observed using direct T_2 measurements, and no systematic differences between the two measurements were found.

Like the other relaxation measurements, the different regions of the peptide exhibit systematic differences in NOE values. The N- and C-terminal residues have negative or low NOE values. The β-strand region has an average NOE value of 0.73 ± 0.02, and the region contacting the switches has an average NOE of 0.63 ± 0.03, with V25 and E28 exhibiting the lowest NOE values of 0.36 and 0.38, respec-

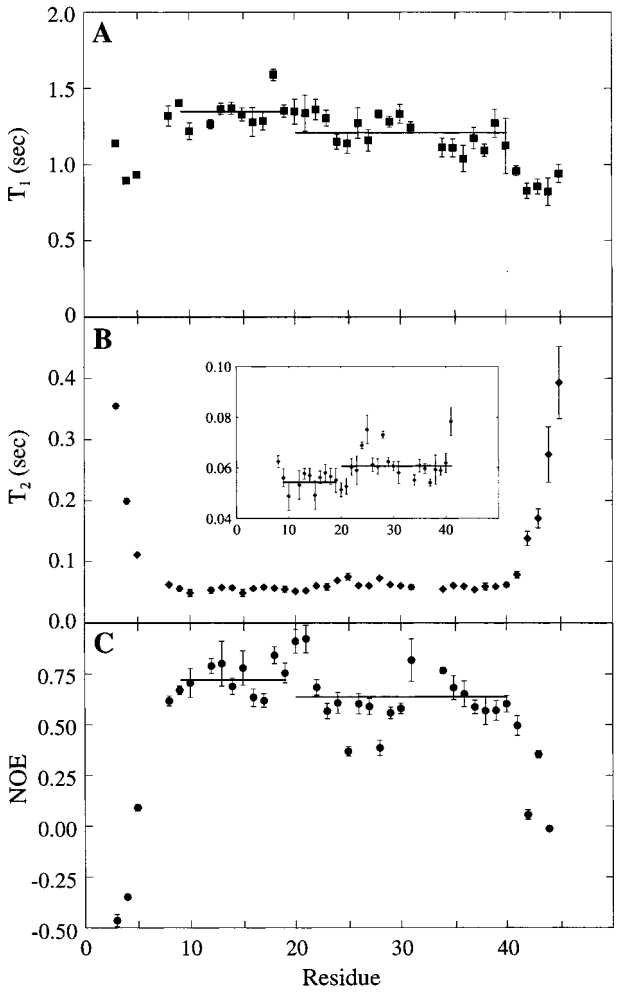

FIGURE 3: Relaxation data at 600 MHz for PBD46 bound to Cdc42Hs·GMPPCP. **(**A**)** Residue-specific spin−lattice relaxation times, T_1. **(**B**)** Residue-specific spin−spin relaxation times, T_2, derived from $T_{1\rho}$ measurements. The inset shows the expanded region of the T_2 plot that does not include the N and C termini. **(**C**)** Residue-specific steady-state NOEs. The horizontal lines in each of the three plots indicate the average values of the relaxation parameters for residues 9−19 and 20−40.

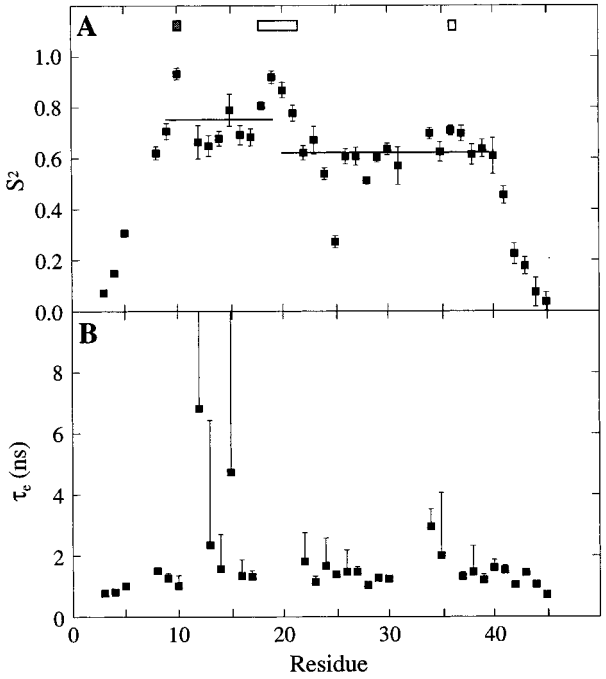

FIGURE 4: Residue-specific dynamics parameters extracted from the extended Lipari−Szabo model-free formalism (*33*) for PBD46 bound to Cdc42Hs·GMPPCP: **(**A**)** order parameters and **(**B**)** local correlation times. In part A, the residues fit best with model 1 are indicated at the top of the plot by an open box, and those fit best by model 2 are shown with a gray box. All others are best fit with model 5. In a few cases (S10, E15, and G31), the best-fit model produced τ_e values that almost reached the value of τ_m and had a very high error, indicating that local motions on a pico- to nanosecond timescale for these residues are difficult to model accurately. The value of τ_e for G31 (14.05 ± 4.79 ns) is off-scale.

tively (Figure 3C). Thus, the three relaxation measurements (T_1, T_2, and NOE) show consistent differences in different regions of the peptide.

Backbone Dynamics. The dynamics model best describing the data for each residue in bound PBD46 is shown in Figure 4A. Residues 18−21 and 36 are fit best with model 1, whereas residue 10 is fit best with model 2. The remaining residues are fit best with model 5, which indicates that the peptide, despite the fact that it is somewhat immobilized in its bound state, exhibits motion on two timescales. None of the residues in the peptide fit either model 3 or model 4, indicating the absence of chemical-exchange processes on the micro- to millisecond timescale.

(a) N and C Termini. The residue-specific order parameters and local correlation times for bound PBD46 are shown in Figure 4. The S^2 values for the N and C termini are smaller than the S^2 values of the other regions of the peptide. This indicates that both the N and C termini exhibit high mobility on the pico- to nanosecond timescale, which is consistent with relatively unstructured portions of the peptide that make minimal contact with Cdc42Hs (*13*).

(b) Residues 9−19 (β-Strand Region). The average S^2 in this region is 0.75 ± 0.03 (average τ_e values of 1.48 ± 0.19 ns, excluding S12 and E15), indicating limited pico- to nanosecond timescale motion. Residues S12 and E15 show long τ_e with large error (Figure 4B), suggesting that these residues may have complex backbone dynamics that were not well-characterized by the models. From the NMR structure (*13*), E15 and T17 make hydrophobic contacts with the conserved residue Y40 in Cdc42Hs. In addition, the carboxyl group of E15 can hydrogen bond with the hydroxyl group of Y40 (Cdc42Hs). These interactions in addition to the hydrogen bonding across the β sheet may restrict the internal motion of this region.

(c) Residues 20−40 (Region That Contacts Switches I and II and the P Loop). The average S^2 value for this region is 0.63 ± 0.03, which indicates that this region has increased mobility relative to the β strand. However, the order parameters vary in this region, depending upon the contact with Cdc42Hs. Those residues in PBD46 near the end of the β strand and in contact with Switch II (residues 19−21) show somewhat decreased mobility and are best fit by model 1 (vs model 5 for most of the remainder of the peptide). This parallels the motional characteristics of Cdc42Hs, which suggest that although Switch II undergoes chemical exchange in the free form, it exhibits a much simpler motion in the bound form (*14*). Also, the Switch II region of the complex of Cdc42Hs·GMPPCP and PBD46 gives rise to more NOEs and a better-defined structure (*13*) than the corresponding region of free Cdc42Hs (*35*). An unusually low-order

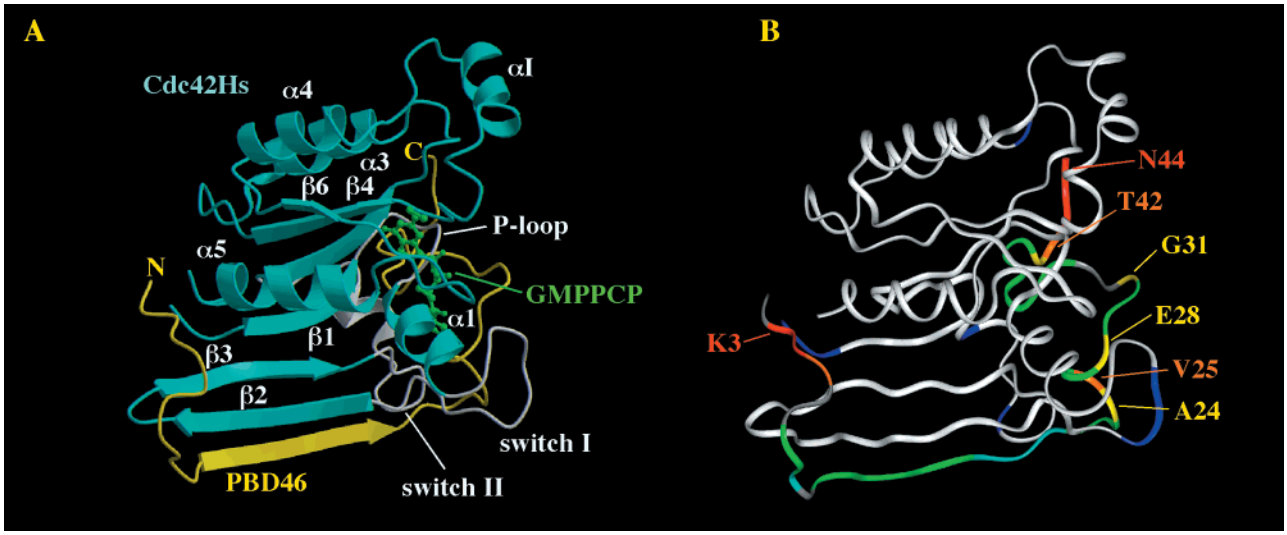

FIGURE 5: **(**A**)** NMR structure of the Cdc42Hs·GMPPCP−PBD46 complex showing the secondary structures of both Cdc42Hs and PBD46. Cdc42Hs is depicted in cyan and PBD46 in yellow. Switch I, Switch II, and the P loop are shown in white, and GMPPCP is shown in green. **(**B**)** Ribbon structure colored according to the order parameters: blue, residues of Cdc42Hs that have S^2 values below 0.8; cyan, residues of PBD46 that have S^2 values above 0.8; green, residues of PBD46 that have S^2 values below 0.8 and above 0.6; yellow, residues of PBD46 that have S^2 values below 0.6 and above 0.4; orange, residues of PBD46 that have S^2 values below 0.4 and above 0.2; red, residues of PBD46 that have S^2 values below 0.2. Residues in PBD46 for which S^2 has not been determined are shown in gray.

parameter has been observed for residue V25 ($S^2 = 0.27 \pm 0.03$). V25 interacts with T35 of Cdc42Hs and is in a region of Cdc42Hs that exhibits significant internal motion, even in the complex with PBD46 (Figure 5B; *14*). Likewise, other residues in close proximity to flexible residues in Switch I also exhibit low-order parameters (A24 and E28). In contrast, several residues in close proximity to the P loop of Cdc42Hs (E34, W36, and A37) exhibit somewhat higher-order parameters, consistent with the lack of motional complexity and high-order parameters in the P loop of bound Cdc42Hs (*14*). The P loop plays an important role in GTP hydrolysis, and the interaction of PBD46 with this region of Cdc42Hs may play a role in restricting the conformational adjustments required for enzymatic activity. Thus, while residues 20−40 have generally lower-order parameters than the β-strand region of PBD46, the order parameters vary according to the dynamics characteristics of the regions of Cdc42Hs with which they make contact.

DISCUSSION

Free PBD46 is highly mobile and unstructured, while PBD46 when bound to Cdc42Hs is less mobile and highly structured. The NMR structure of the Cdc42Hs·GMPPCP−PBD46 complex (*13*) shows that the binding of PBD46 to Cdc42Hs encompasses a large surface area interacting with Switches I and II, the P loop, α1, and α5 of Cdc42Hs (Figure 5). In addition, PBD46 forms an antiparallel β sheet with the β2 strand of Cdc42Hs. The extensive binding surface between PBD46 and Cdc42Hs can account for the high affinity of the complex and the effects of PBD46 on both the GDP−GTP exchange rate and the rate of GTP hydrolysis (*12*). This is reflected in the significant negative enthalpic component of binding ($\Delta H = -13.0$ kcal/mol, $\Delta G = -10.6$ kcal/mol; *36*) accompanied by entropic loss associated with loss of internal motion in both Cdc42Hs and PBD46 upon complex formation ($T\Delta S$ of −2.4 kcal/mol at 25 °C; *36*). However, the net entropic loss is in part a balance between the loss of entropy due to a restriction of the backbone and the increase in entropy due to an increased flexibility of the side-chain methyls in the complex (*15*).

Here, we have shown that bound PBD46 exhibits significantly different dynamic properties (Table 2) in the regions of the peptide that interact with different structural regions of Cdc42Hs (*13*). The N- and C-terminal regions of the bound peptide have low-order parameters (which suggests that these regions of the peptide experience high-amplitude motion on a pico- to nanosecond timescale). This is consistent with the structure of the complex, which indicates little or no interaction between Cdc42Hs and the termini of the peptide. The one exception to this is K3 of PBD46, which does interact with two leucines (L174 and L177) near the C-terminal end of the α5 helix of Cdc42Hs (*13*). However, this interaction occurs through relatively long side chains so that the N−H bond vector of this residue could maintain high flexibility while interacting significantly at the side chains.

In contrast, the β-strand region (residues 9−19) exhibits order parameters higher than those of the other regions of the peptide. The relatively low mobility of this region can be attributed to the antiparallel β sheet that is formed with the β2 strand of Cdc42Hs. In the absence of PBD46, the β2 strand of Cdc42Hs is somewhat more mobile than the remainder of the β sheet (models 2 and 5; *14*). Upon binding to PBD46, β2 is fit exclusively with model 1, and the order parameters increase slightly (*14*). Significantly, residues in Switch I and extending to the N-terminal end of β2 are not observed in the unbound form of Cdc42Hs (apparently because of exchange broadening) but are clearly observed upon PBD46 binding (*12*). Thus, the binding of PBD46 seems to decrease the internal backbone motions of the β2 strand of Cdc42Hs. Furthermore, the reduced motion of β2 is reflected in the reduced motion of PBD46 in this region.

Beyond the β-strand region of PBD46 (residues 23−31, V25 in particular), the bound peptide exhibits increased internal motion. In general, these residues are in close proximity to Switch I of Cdc42Hs. Figure 5B shows both

Cdc42Hs and PBD46, colored according to the order parameters. It is interesting to note that, excluding the termini of both proteins, the regions showing the lowest-order parameters in both Cdc42Hs and PBD46 in the complex are in close contact. Switch I of Cdc42Hs is a highly mobile region of the protein (*14*), and it is this part of the protein that has extensive interactions with different effectors (e.g., ACK, WASP, and PBD46) and regulatory proteins (e.g., GDI and GAP). Because this region of Cdc42Hs remains mobile in the complex with PBD46 (*14*), PBD46 and Cdc42Hs are likely to move in concert. Changes in the internal dynamics of proteins upon complex formation have important consequences for the binding energies of the interaction and associated conformational changes. Given the dynamic behavior of the two free species and the concerted motion of the bound complex, the two species have adapted to each other to form a low-energy, induced-fit conformation. Considering the role of flexibility and the concerted motion of the bound complex, one prediction would be that restricting the number of conformations available to Switch I or Switch II may modify the affinity or block the binding of effectors. Thus, mutations that affect the flexibility of Switch I might alter the energy landscape such that effector binding is diminished or eliminated.

Although some similarities exist between the NMR structure of the bound PBD46 (*13*) and the crystal structure of isolated PAK1 (*11*), such as a β strand in the same region (Figure 1), the NMR data show the presence of neither the β hairpin, the second β strand, nor the helix that are present in the isolated PAK structure. In particular, the chemical shift index, H−D exchange rates, and lack of diagnostic NOEs indicate the absence of a helix in the bound structure of Cdc42Hs−PBD46 (only one NOE was observed that would be consistent with a helix in the region of PBD46 (residues 33−44) that corresponds to the helix in PAK1 (residues 100−111), and neither the chemical shift index nor the H−D exchange are consistent with a helical structure; *13*). Our dynamics studies on bound PBD46 support the absence of a helical structure, because low-order parameters were observed particularly for residues 40−45 which includes the region of PAK1 that exhibits a helical structure. Recently, Morreale et al. (*18*) reported an NMR structure of the complex between Cdc42Hs and another PAK fragment (residues 75−118). The 75−118 PAK peptide (Figure 1) is longer at the C terminus (an additional five residues) but shorter by five residues at the N terminus as compared to PBD46. Their analysis indicates that, like the isolated PAK1, residues 100−108 (which are equivalent to residues 33−41 in PBD46) form a helical structure in both the free and bound peptide. The 75−118 PAK peptide binds with a lower affinity than PBD46 (K_D of 16 nM (*12*) vs 120 nM; *37*), and the difference in affinity seems to be due to the truncation at the N-terminal end (*12*). Previously Abdul-Manan et al. (*20*) studied the NMR structure of Cdc42Hs and WASP−GBD. Again, a helical structure in the C terminus of the bound WASP−GBD (WASP−GBD·Cdc42 complex) was observed. However, neither free nor bound fACK forms a helical structure in the C terminus (*19*). Both PBD46 and fACK are shorter **(**Figure 1) at the C terminal as compared to WASP−GBD and PAK (residues 75−118), but both exhibit binding affinities as high as or higher than WASP−GBD and PAK (75−118; *19*). It has been shown that including additional residues from PAK at the C terminus of PBD46 does not increase the binding affinity (*12*). Thus, although the helix may be present in the Cdc42Hs−PAK1 complex, it is unlikely that the helical structure contributes significantly to the binding energy.

Kim et al. (*38*) have studied the autoinhibition and activation mechanisms of WASP and have shown that WASP−GBD, which is largely unstructured in the free state, can be induced to form a compact, folded domain structure by binding to its own VCA domain (a WASP region that interacts with actin and Arp2/3) or by adding a small amount of organic solvent to stabilize the secondary structure. It was suggested that the binding of Cdc42Hs (in a manner that is competitive with VCA) causes a structural transition in WASP that results in the dissociation of its intramolecular contacts and enhanced Arp2/3-mediated actin polymerization. Likewise, the dimerization region of PAK1 (which includes the CRIB sequence and encompasses PBD46) and a nearby inhibitory switch are thought to lose the dimeric and internal contacts in order to associate with Cdc42Hs. This removal of the internal contacts between the inhibitory switch and the kinase domain activates PAK1 (*11*). It is possible that an intermediate step in this process would be a largely unstructured dimerization domain, which would subsequently bind to Cdc42Hs. This interaction would be analogous to the interaction between Cdc42Hs and the free, unstructured form of PBD46, suggesting that the two binding surfaces form as an induced fit. The flexibility of Cdc42Hs at the binding interface is characteristic of the interaction surface of many proteins (*39*). Determining the characteristics of the dynamics of both binding partners in the bound and free states adds an important component to our understanding of protein−protein interactions and is essential information in cases where the inhibition of binding may lead to new therapeutic agents.

SUMMARY

Free PBD46 is highly mobile and unstructured, but its mobility decreases and it becomes highly structured when bound to Cdc42Hs·GMPPCP. Different dynamics characteristics have been observed in the different regions of PBD46 bound to Cdc42Hs. Both the N and C termini are highly mobile, mirroring the weak interaction with Cdc42Hs (*13*). However, the β-strand region shows a high degree of local order in the pico- to nanosecond timescale, reflecting the high-order parameters observed for the corresponding region on Cdc42Hs (the β2 strand; *14*). Residues 23−31 exhibit increased mobility relative to the β-strand region; in particular, V25 has a low-order parameter and interacts with a particularly mobile region of Cdc42Hs (Switch I). This mobile region, which exists as a helix in isolated PAK1 (residues 33−44), exhibits somewhat lower-order parameters than the β-strand region in PBD46 and does not appear to be helical. Because PBD46 binds Cdc42Hs with high affinity, the absence of a helical structure in bound PBD46 indicates that the contribution of this helix to the binding energy may not be significant. The dynamic behavior of free PBD46 and Cdc42Hs and the concerted motion of the bound complex are consistent with an induced-fit model by which the two species form a tight, low-energy configuration.

ACKNOWLEDGMENT

We are grateful to Dr. Lewis Kay (University of Toronto) for making available the pulse sequences that were used and Dr. Arthur Palmer (Columbia University) for the model-free program. We thank Dr. Linda Nicholson (Cornell University) for the program (Quick) that was used to perform an exponential fit of the relaxation data. We thank the laboratory of Chemical Physics at the National Institutes of Health and Drs. Dan Garrett and Frank Delaglio for making the programs PIPP and NMRPipe available, which were useful in analyzing our NMR data. We thank Dr. Adrienne Loh (University of Wisconsin, La Crosse), Dr. Paul Adams, Rob McFeeters, and Dr. Gregory Weiland for helpful discussions.

REFERENCES

1. Bourne, H. R., Sanders, D. A., and McCormick, F. (1991) *Nature 349*, 117−127.
2. Bredel, M., and Pollack, I. (1999) *Brain Res. Rev. 29*, 232−249.
3. Zheng, Y., Bagrodia, S., and Cerione, R. A. (1994) *J. Biol. Chem. 269*, 18727−18730.
4. Aspenstrom, P., Lindberg, U., and Hall, A. (1996) *Curr. Biol. 6*, 70−75.
5. Manser, E., Leung, T., Salihuddin, H., Tan, L., and Lim, L. (1993) *Nature 363*, 364−367.
6. Bagrodia, S., Taylor, S., Creasy, C., Chernoff, J., and Cerione, R. (1995) *J. Biol. Chem. 270*, 22731−22737.
7. Manser, E., Leung, T., Salihuddin, H., Zhao, Z., and Lim, L. (1994) *Nature 367*, 40−46.
8. Burbelo, P. D., Drechsel, D., and Hall, A. (1995) *J. Biol. Chem. 270*, 29071−29074.
9. Lim, L., Manser, E., Leung, T., and Hall, C. (1996) *Eur. J. Biochem. 242*, 171−185.
10. Sells, M. A., and Chernoff, J. (1997) *Trends Cell Biol. 7*, 162−167.
11. Lei, M., Lu, W., Meng, W., Parrini, M.-C., Eck, M. J., Mayer, B. J., and Harrison, S. C. (2000) *Cell 102*, 387−397.
12. Guo, W., Sutcliffe, M. J., Cerione, R. A., and Oswald, R. E. (1998) *Biochemistry 37*, 14030−14037.
13. Gizachew, D., Guo, W., Chohan, K. K., Sutcliffe, M. J., and Oswald, R. E. (2000) *Biochemistry 39*, 3963−3971.
14. Loh, A. P., Guo, W., Nicholson, L. K., and Oswald, R. E. (1999) *Biochemistry 38*, 12547−12557.
15. Loh, A., Pawley, N., Nicholson, L. K., and Oswald, R. E. (2001) *Biochemistry 40*, 4590−4600.
16. Shinjo, K., Koland, J. G., Hart, M. J., Narasimhan, V., Johnson, D. I., Evans, T., and Cerione, R. A. (1990) *Proc. Natl. Acad. Sci. U.S.A. 87*, 9853−9857.
17. John, J., Sohmen, R., Feurstein, J., Linke, R., Wittinghofer, A., and Goody, R. S. (1990) *Biochemistry 29*, 6058−6065.
18. Morreale, A., Venkatesan, M., Mott, H. R., Owen, D., Nietlispach, D., Lowe, P. N., and Laue, E. D. (2000) *Nature Struct. Biol. 7*, 384−388.
19. Mott, H. R., Owen, D., Nietlispach, D., Lowe, P. N., Manser, E., Lim, L., and Laue, E. D. (1999) *Nature 399*, 384−8.
20. Abdul-Manan, N., Aghazadeh, B., Liu, G. A., Majumdar, A., Ouefelli, O., Siminovich, K. A., and Rosen, M. K. (1999) *Nature 399*, 379−383.
21. Marion, D., Driscoll, P. C., Kay, L. E., Wingfield, P. T., Bax, A., Gronenborn, A., and Clore, G. M. (1989) *Biochemistry 28*, 6150−6156.
22. States, D. J., Haberkorn, R. A., and Ruben, D. J. (1982) *J. Magn. Reson. 48*, 286−292.
23. Kay, L. E., Keifer, P., and Saarinen, T. (1992) *J. Am. Chem. Soc. 114*, 10663−10665.
24. Delaglio, F., Grzesiek, S., Vuister, G., Zhu, G., Pfeifer, J., and Bax, A. (1995) *J. Biomol. NMR 6*, 277−293.
25. Kay, L. E., Nicholson, L. K., Delaglio, F., Bax, A., and Torchia, D. A. (1992) *J. Magn. Reson. 97*, 359−375.
26. Farrow, N. A., Muhandiram, R., Singer, A. U., Pascal, S. M., Kay, C. M., Gish, G., Shoelson, S. E., Pawson, T., Forman-Kay, J. D., and Kay, L. E. (1994) *Biochemistry 33*, 5984−6003.
27. Peng, J. W., Thanabal, V., and Wagner, G. (1991) *J. Magn. Reson. 95*, 421−427.
28. Nicholson, L. K., Grzesiek, S., Yamazaki, T., Stahl, S. J., Kaufman, P. T., Wingfield, P. T., Domaille, P. J., Bax, A., and Torchia, D. A. (1995) *Nature Struct. Biol. 2*, 274−280.
29. Davis, D. G., Perlman, M. E., and London, R. E. (1994) *J. Magn. Reson. B104*, 266−275.
30. Nicholson, L. K., Kay, L. E., Baldisseri, D. M., Arango, J., Young, P. E., Bax, A., and Torchia, D. A. (1992) *Biochemistry 31*, 5253−5263.
31. Abragam, A. (1961) *Principles of Nuclear Magnetism*, Clarendon Press, Oxford.
32. Lipari, G., and Szabo, A. (1982) *J. Am. Chem. Soc. 104*, 4559−4570.
33. Clore, G. M., Driscoll, P. C., Wingfield, P. T., and Gronenborn, A. M. (1990) *Biochemistry 29*, 7387−401.
34. Palmer, A. (1998) ModelFree Version 4.0, http://cpmcnet.columbia.edu/dept/gsas/biochem/labs/palmer.
35. Feltham, J. L., Dötsch, V., Raza, S., Manor, D., Cerione, R. A., Sutcliffe, M. J., Wagner, G., and Oswald, R. E. (1997) *Biochemistry 36*, 8755−8766.
36. Guo, W. (2000) Ph.D. Thesis, Cornell University, Ithaca, NY.
37. Thompson, G., Owen, D., Chalk, P. A., and Lowe, P. N. (1998) *Biochemistry 37*, 7885−91.
38. Kim, A. S., Kakalis, L. T., Abdul-Manan, N., Liu, G. A., and Rosen, M. K. (2000) *Nature 404*, 151−158.
39. Luque, I., and Freire, E. (2000) *Proteins 40*, 63−71.

BI010989H